https://doi.org/10.5194/egusphere-2023-506
Preprint. Discussion started: 3 April 2023
© Author(s) 2023. CC BY 4.0 License.

The response of wildfire regimes to Last Glacial Maximum carbon dioxide and climate

Olivia Haas[1,2], Iain Colin Prentice[1,2], Sandy P. Harrison[1,3]

[1]Leverhulme Centre for Wildfires, Environment and Society, Imperial College London, South Kensington, London SW7 2BW, UK

[2]Georgina Mace Centre for the Living Planet, Department of Life Sciences, Imperial College London, Silwood Park Campus, Buckhurst Road, Ascot SL5 7PY, UK

[3]Geography & Environmental Science, University of Reading, Whiteknights, Reading RG6 6AH, UK

Correspondence to: Olivia Haas (o.haas20@imperial.ac.uk)

Abstract

Climate and fuel availability jointly control the incidence of wildfires. The effects of atmospheric CO_2 on plant growth influence fuel availability independently of climate; but the relative importance of each in driving large-scale changes in wildfire regimes cannot easily be quantified from observations alone. Here, we use previously developed empirical models to simulate the global spatial pattern of burnt area, fire size and fire intensity for modern and Last Glacial Maximum (LGM; ~ 21,000 ka) conditions using both realistic changes in climate and CO_2 and sensitivity experiments to separate their effects. Three different LGM scenarios are used to represent the range of modelled LGM climates. We show large, modelled reductions in burnt area at the LGM compared to the recent period, consistent with the sedimentary charcoal record. This reduction was predominantly driven by the effect of low CO_2 on vegetation productivity. The amplitude of the reduction under low CO_2 conditions was similar regardless of the LGM climate scenario and was not observed in any LGM scenario when only climate effects were considered, with one LGM climate scenario showing increased burning under these conditions. Fire intensity showed a similar sensitivity to CO_2 across different climates but was also sensitive to changes in vapour pressure deficit (VPD). Modelled fire size was reduced under LGM CO_2 in many regions but increased under LGM climates because of changes in wind strength, dryness (DD) and diurnal temperature range (DTR). This increase was offset under the coldest LGM climate in the northern latitudes because of a large reduction in VPD. These results emphasis the fact that the relative magnitudes of changes in different climate variables influence the wildfire regime and that different aspects of climate change can have opposing effects. The importance of CO_2 effects imply that future projections of wildfire must take rising CO_2 into account.

1. Introduction

Climate influences the occurrence of wildfires both through fire weather, which affects the probability of wildfire start and spread, and the long-term establishment of vegetation which is strongly controlled by temperature and precipitation (Bradstock, 2010; Pausas & Ribeiro, 2013). It has been suggested that current climate change, driven by increasing atmospheric CO_2 levels, will increase wildfire risk in many regions through increased fuel dryness whilst potentially reducing wildfire risk in some regions due to decreasing fuel availability (e.g. Abatzoglou et al., 2019a; Bowman et al., 2020; Harrison et al., 2021; Rogers et al., 2020). However,

https://doi.org/10.5194/egusphere-2023-506
Preprint. Discussion started: 3 April 2023
© Author(s) 2023. CC BY 4.0 License.

atmospheric CO_2 levels also affect fuel loads independently of climate through physiological effects on photosynthesis which cascade into plant growth rates (Bond et al., 2003; Bond & Midgley, 2012; Kgope et al., 2010). Much emphasis has been placed on recent and future changes in fire weather (see e.g. Abatzoglou et al., 2019; Betts et al., 2015; Flannigan et al., 2013; Jolly et al., 2015). However, increases in atmospheric CO_2 concentrations promote vegetation productivity, thus altering fuel availability and loads, as well as affecting fuel types through e.g. woody thickening (Buitenwerf et al., 2012; Donohue et al., 2013; Knorr et al., 2016; Martin Calvo et al., 2014; Martin Calvo & Prentice, 2015; Pausas, 2015). Fuel properties have different effects on different aspects of the fire regime, with fire size strongly constrained by fuel continuity and fire intensity limited by fuel loads (Archibald et al., 2013; Haas et al., 2022). Thus, CO_2-induced changes in vegetation properties will most likely affect these aspects of wildfire regimes differently.

One reason the impact of CO_2 on wildfires is poorly constrained is the difficulty of isolating it based on observations alone. Satellite records only span ~25 years, a relatively short period to monitor the effect of changing CO_2 levels on the vegetation properties that influence wildfires. Furthermore, changes in atmospheric CO_2 levels and climate are temporally correlated, and since both affect vegetation, it difficult to attribute changes in observations to one or the other. An alternative approach is to use process-based fire-enabled vegetation models which explicitly account for the physiological effects of CO_2 and can be used to examine the temporal and spatial patterns of wildfires under different conditions. Process-based models have been used to examine the impact of climate and atmospheric CO_2 changes on both vegetation and wildfire at the last glacial maximum (LGM; 21,000 years ago) (Martin Calvo et al., 2014; Martin Calvo & Prentice, 2015). The LGM is a useful out-of-sample experiment since the climate forcing is of similar magnitude as the change expected by the end of the century in high-end scenarios, though of opposite sign (Kageyama et al., 2021). The LGM had a generally colder and drier climate than today, with CO_2 levels ~ 185 ppm. Palaeorecords show reduced vegetation productivity and forest cover (Harrison & Prentice, 2003; Kaplan et al., 2016; Moreno et al., 2018), and ice core and sedimentary charcoal records indicate reduced biomass burning globally (Albani et al., 2018; Harrison et al., 2022; Marlon et al., 2016; Rubino et al., 2016). Although this reduction could reflect the colder and drier conditions, model experiments suggests that low CO_2 also played a crucial role. Experiments using the coupled biogeography and biogeochemistry model BIOME4 (Kaplan et al., 2003) showed that it was necessary to include the direct effect of CO_2 to simulate observed global and regional reduction in forest cover during the glacial (Bragg et al., 2013; Harrison & Prentice, 2003). Similarly, Martin Calvo et al. (2015) showed that low CO_2 was necessary to simulate the observed reduction of biomass burning in LGM experiments using the LPX fire-enabled vegetation model.

In this analysis, we use three empirical models (Haas et al., 2022)to explore the relative importance of climate and of CO_2 on the global spatial patterns of burnt area, fire size and fire intensity. We performed two experiments under realistic modern CO_2 and climate conditions (MOD climate/MOD CO_2 and LGM climate/LGM CO_2). We also performed two counterfactual sensitivity experiments to quantify the sensitivity of each wildfire property to climate and CO_2 independently (MOD climate/LGM CO_2 and LGM climate/MOD CO_2). Comparisons to LGM charcoal records from the Reading Palaeofire Database (RPD) (Harrison et al., 2022) were used to examine which experiments provided the most realistic spatial patterns.

https://doi.org/10.5194/egusphere-2023-506
Preprint. Discussion started: 3 April 2023
© Author(s) 2023. CC BY 4.0 License.

2. Methods

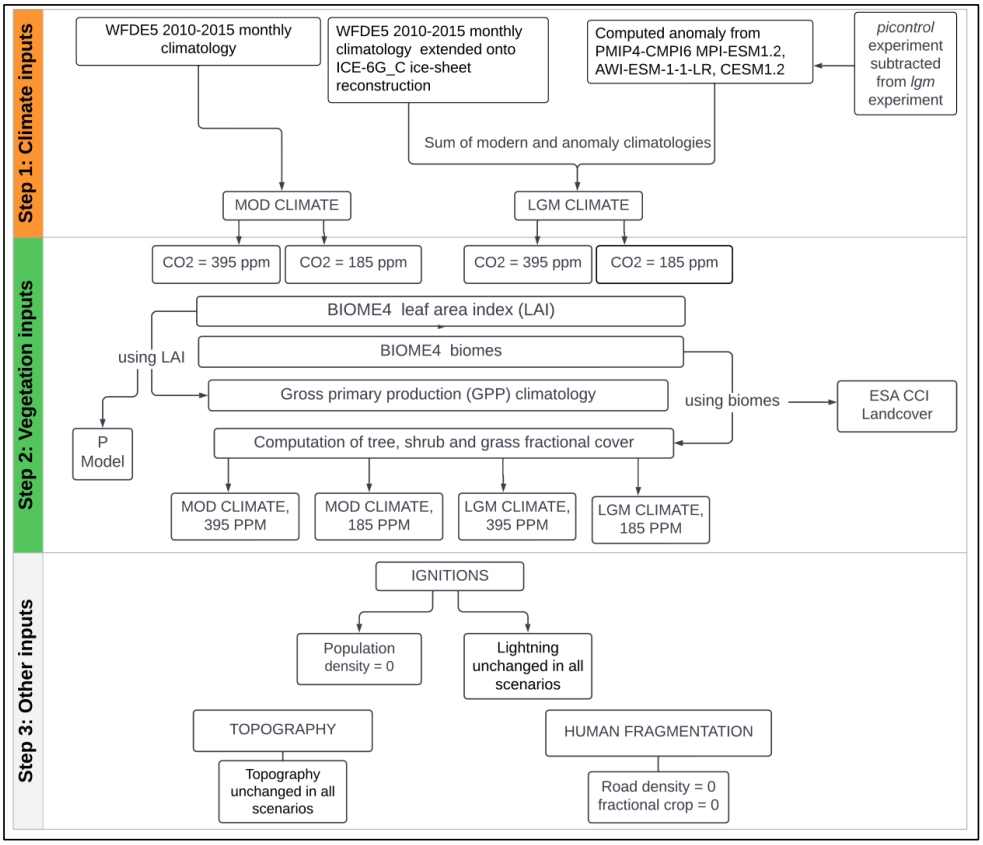

Figure 1. Flowchart of the method to obtain each of the four scenarios: MOD climate and MOD CO_2, LGM climate and LGM CO_2, MOD climate and LGM CO_2 and LGM climate and LGM CO_2.

The empirical models were developed by applying generalised linear modelling (GLM) to modern observations (Haas et al., 2022) to simulate the global spatial patterns of burnt area (BA), fire size (FS) and fire intensity (FI) under four climate/CO_2 scenarios (Figure 1). We used two realistic scenarios: (a) MOD climate and CO_2 conditions and (b) LGM climate and CO_2. We ran two sensitivity experiments (a) combining MOD climate and LGM CO_2 and (b) combining LGM climate and MOD CO_2 levels. The empirical models use climate, vegetation, topography, lightning ignitions, land cover, road density and human population density as predictors to represent the environmental controls on each of the wildfire properties.

Modern (MOD) climate data (daily temperature (T), daily precipitation (P), photosynthetic photon flux density (PPFD), monthly wind speeds (wind), vapour pressure deficit (VPD), monthly specific humidity (huss), cloud cover (cld), monthly pressure (Pa)) were obtained from the WFDE5 bias-adjusted ERA5 database (Cucchi et al., 2020) for 2010 to 2015. Following the methodology in Haas et al. (2022), the number of monthly dry days (DD) and monthly diurnal temperature range (DTR) were calculated. Seasonal climatologies were derived for all variables eliminating inter-annual variability. For each grid cell, values from the month with (on average) the

https://doi.org/10.5194/egusphere-2023-506
Preprint. Discussion started: 3 April 2023
© Author(s) 2023. CC BY 4.0 License.

maximum number of DD, the largest DTR, and the highest VPD were selected. Wind speed value was taken from the hottest month of the year (determined from the WFDE5 2 m air temperature (Cucchi et al., 2020)). For lightning, the mean value over the seasonal climatology was selected. A seasonality predictor to account for wet vs dry seasons was constructed by dividing the range of monthly values from the seasonal DD climatology by the mean value of all 12 months. Expanded ice sheets in North America, Fennoscandia, Greenland, and Antarctica resulted in global sea levels ~ 120 m lower than today at the LGM. The modern climate data were extrapolated out onto the exposed shelves using the ICE-6G_C (Peltier et al., 2015) boundary conditions and a nearest neighbour approach from the *GeoInterpolation* package in R.

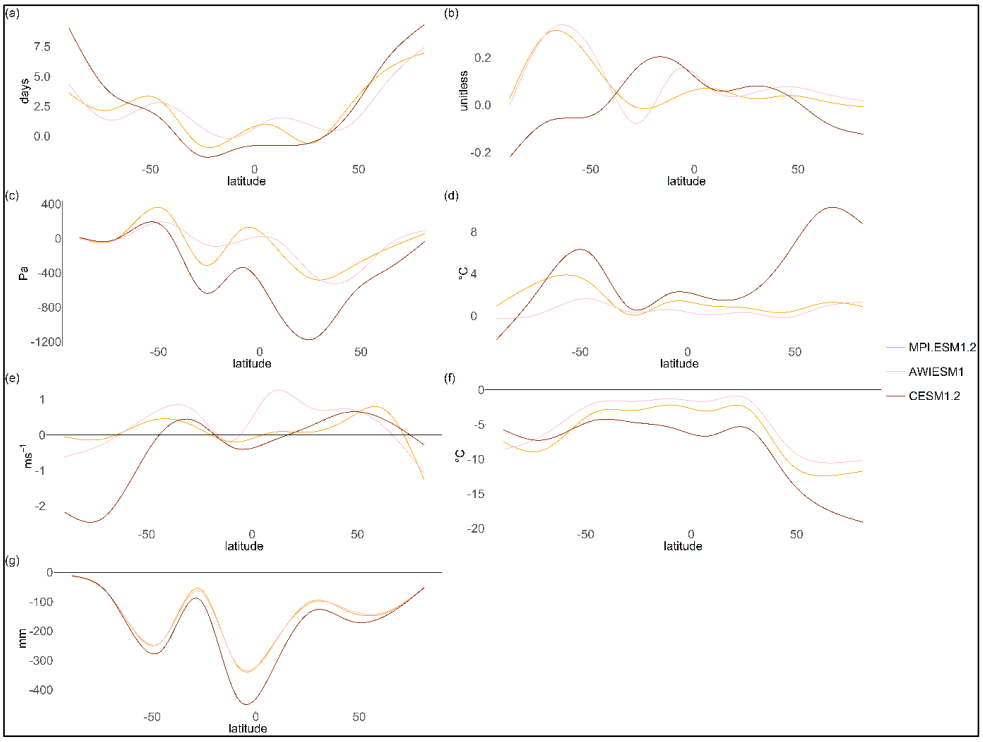

Figure 2. Latitudinal distribution of the LGM-MOD anomalies for MPI.ESM1.2 (orange), AWI-ESM1.2 (pink) and CESM1.2 (brown) for (a) the maximum number of dry days, (b) the seasonality of dry days, (c) maximum monthly VPD, (d) maximum monthly DTR, (e) maximum monthly mean wind speeds, (f) mean monthly temperature and (g) mean monthly total precipitation. The zero-intercept line represents no change between LGM and MOD climate, with negative values representing lower values at the LGM and positive values representing higher values at the LGM.

LGM climate data were obtained from three models participating in the Palaeoclimate Modelling Intercomparison Project (PMIP) contribution to the sixth phase of the Coupled Model Intercomparison Project (CMIP6), AWI-ESM-1-1-LR (short name: AWIESM1) (Lohmann et al., 2020; Sidorenko et al., 2015),

https://doi.org/10.5194/egusphere-2023-506
Preprint. Discussion started: 3 April 2023
© Author(s) 2023. CC BY 4.0 License.

MPI_ESM1.2 (Mauritsen et al., 2019), CESM1.2 (F. Li et al., 2013; Tierney et al., 2020) to represent a range of LGM climates (Figure 2). A seasonal climatology was derived for each climate variable from the PMIP *picontrol* experiment (pre-industrial conditions, PI) and the PMIP *lgm* experiment of the PMIP4-CMIP6 simulations. The difference between the PI and LGM values (PI-LGM anomalies) were calculated and added to the MOD climatology (see Figure 1). The use of anomalies is designed to minimise the impact of systematic model biases on the derived climate. This approach provided three LGM climate scenarios, resulting in nine experiments for BA, FS and FI respectively.

We obtained MOD and LGM vegetation and gross primary production (GPP) using the coupled biogeography and biogeochemistry model BIOME4 (Kaplan et al., 2003) and a simple optimality-based model of GPP, the P Model (Wang et al., 2017; Stocker et al., 2020). BIOME4 was used to simulate biome distribution with modern day climate data (T, P, cld) setting CO_2 levels to 395 ppm (the annual mean from 2010-2015) and 185 ppm in turn. LGM biome distributions were simulated using the three different LGM scenarios, again setting CO_2 levels to 395 ppm and 185 ppm respectively. We derived mean fractional tree, shrub, and grass cover for each of these nine experiments using the mean values for each biome from ESA CCI Landcover (W. Li et al., 2018). We also calculated fAPAR for each experiment from the leaf area index (LAI) computed by BIOME4 and obtained fractional cover of C_4 plants (see S1). We computed global monthly C_3 and C_4 photosynthesis using the P model using appropriate combinations of climate (T, VPD, ppfd and Pa), BIOME4-derived fAPAR and CO_2 concentration for the MOD and LGM scenarios (see Figure 1). Total GPP was calculated as:

$$GPP_{monthly} = GPP_{c3}\left(1 - C4_{fraction}\right) + GPP_{c4}C4_{fraction}\ , \qquad (1)$$

with GPP_{c3} and GPP_{c4} representing monthly C_3 and C_4 GPP values from the P Model and $C4_{fraction}$ representing the fractional C4 cover from BIOME4 (see Table1).

Scenario	Modern climate	MPI_ESM1.2	AWIESM1	CESM1.2 LGM
Modern CO_2 (395 ppm)	149.37	106.63	112.06	88.44
LGM CO_2 (185 ppm)	66.54	55.49	69.61	50.37

Table 1. Total annual gross primary production (GPP) (in PgC) estimates for each scenario.

This approach led to estimates of total BA, median FS, and median FI under modern conditions of a similar magnitude to the original GLM models and other global estimates (Andela et al., 2019; Humber et al., 2019) (Table 2).

Topographic and lightning variables were assumed not to change dramatically between the LGM and the present day. We used modern values, extrapolated out onto the exposed shelves, for the LGM experiments. The original GLM models (Haas et al., 2022) included predictors associated with human activity, specifically road density, cropland cover and population density. However, since there was no agriculture at the LGM and the human impact on the natural landscape was slight and relatively localised (Fuller et al., 2014), we excluded these predictors in all the experiments by setting them to 0. This also ensured observed differences between the experiments were driven solely by climate and CO_2. Exclusion of predictors related to human activity increases BA and FS in the original GLM models and produces an even larger increase when changes in vegetation are

https://doi.org/10.5194/egusphere-2023-506
Preprint. Discussion started: 3 April 2023
© Author(s) 2023. CC BY 4.0 License.

considered through using the BIOME4 derived vegetation (Table 2). The effect was negligible for FI, highlighting the sensitivity of BA and FS to human activity.

Inputs for land cover and P Model GPP (Cucchi et al., 2020)	**ESA CCI Landcover NASA/GIMS fAPAR 3g**	**BIOME4 (Kaplan et al., 2003)**	**Global estimates from the literature**
Burnt area (millions km²)			
Human activity on	4.42	4.25	[1.87 – 4.6] (Humber et al., 2019)
Human activity off	7.41	11.27	
Fire size (km²)			
Human activity on	3.36	3.61	4.4 (Andela et al., 2019) (does not include wildfires smaller than 0.21 km²)
Human activity off	5.34	6.25	
Fire intensity (W.km⁻¹)			
Human activity on	40.00	31.41	
Human activity off	39.20	31.17	

Table 2. Sensitivity of GLM models to human activity using both observations and BIOME4 derived vegetation and GPP.

When modelled GPP values were 0, BA, FS and FI was automatically set to 0. Modelled BA values smaller than 0.001 were assumed to imply no burning, thus under these conditions FS and FI were also assumed to be 0 since both GLM models were trained on data of existing fires (see S2). We used the sensitivity experiments to quantify the separate effects of CO_2 and climate on BA, FS and FI independently. We then used the realistic experiments to identify which predictors were driving the largest change between MOD and the three LGM scenarios by excluding one predictor at a time from the GLM models, re-running the LGM experiments and identifying which excluded variable caused the greatest change in the MOD-LGM anomaly in each grid-cell. Comparing these results to the MOD-LGM anomalies allowed us to determine if the predictor was responsible for an increase or a decrease in BA, FS and FI.

We also compared the spatial patterns of BA, FS and FI with sedimentary charcoal data from the Reading Palaeofire Database (RPD; Harrison et al., 2022). Sedimentary charcoal records provide a record of fire activity but may reflect changes in both burnt area or completeness of combustion (Power et al., 2008) so this comparison allowed us firstly to establish which of the fire regimes properties was most closely reflected in these records and secondly which of the scenarios produced the most realistic patterns of burning. Model outputs and the charcoal records were re-gridded to the coarsest resolution of the three climate models (2.5° x 1.875° resolution). We calculated the number of correctly predicted anomalies (same sign within a given grid-cell), separating positive and negative anomalies to assess the rate of false positives as well as false negatives for each scenario and each LGM climate scenario.

https://doi.org/10.5194/egusphere-2023-506
Preprint. Discussion started: 3 April 2023
© Author(s) 2023. CC BY 4.0 License.

3. Results

Global BA was substantially reduced compared to the realistic MOD scenario under all three realistic LGM scenarios, decreasing by 72% for the coldest CESM1.2 LGM scenario, 62% for the MPI-ESM1.2 LGM scenario and 41% for the warmest AWIESM1 LGM scenario. The largest decreases were observed in sub-Saharan Africa (excluding the tropical regions) as well as northern Australia and the Indian subcontinent (MPI-ESM1.2 and CESM1.2 LGM scenarios). Some increases in BA were observed in Alaska (MPI-ESM1.2 and AWIESM1 LGM scenarios) as well as south-East Asia, Indonesia, Papua-New-Guinea, and the northern tip of Australia. Increases in Somalia and Central America were also observed (MPI-ESM1.2 and AWIESM1 LGM scenarios). The number of grid cells (excluding ice covered cells) in which no burning occurred was 3 times higher in the MPI-ESM1.2 and AWIESM1 LGM scenarios and 4 times higher in the CESM1.2 LGM scenario compared to the realistic MOD scenario. This was driven by the expansion of desert and tundra biomes at the LGM. The Arabian plate, Middle East, inland China and Australia, and the tips of South America and Africa saw burning reduced to zero. Nearly all burning above 60°N was excluded, except for Alaska under the MPI-ESM1.2 and AWIESM1 LGM scenarios, with the exclusion extending down to 50°N for the CESM1.2 LGM scenario (see S3).

Globally, there was a large decrease in global median FS and FI when considering all grid-cells (not covered in ice) because of overall global reduction in burning. Under all three LGM scenarios, global median FS and FI were reduced to 0 compared to ~5km^2 for FS and 40W.km^2 for FI. However, when excluding grid-cells in which no burning occurred, both global median FS increased compared to the realistic MOD scenario (by ~16% under the two less conservative scenarios (MPI-ESM1.2 and AWIESM1) and by 12% under the CESM1.2 LGM scenario). The main increases in FS occurred in the Central America, Amazonia, tropical Africa as well as the Indian Subcontinent and Europe and Asia between 30°N and 60°N (except for CESM1.2 which had very few positive anomalies with FS). The largest reductions were observed North America, southern Australia, Middle East, and the rest of Eurasia. Global median FI also increased in regions that were burning under two of the LGM scenarios, by 11% under the CESM1.2 LGM scenario and by 4% for MPI.ESM1.2 LGM scenario. Under the AWIESM1 LGM scenario global median FI decreased by 2% even when excluding grid-cells that were not burning. Despite this, changes in FI were spatially consistent across all three LGM scenarios, with increases in FI occurring primarily across the American and African continents, as well as the Mediterranean Basin and Europe and decreases occurring in Asia and inland Australia.

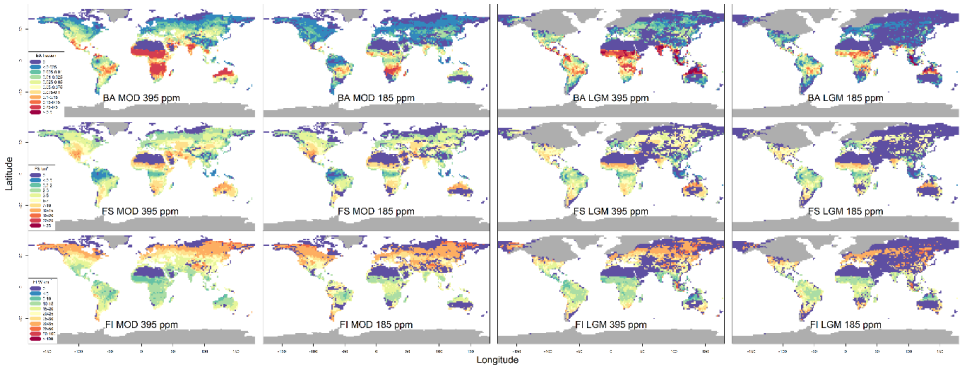

https://doi.org/10.5194/egusphere-2023-506
Preprint. Discussion started: 3 April 2023
© Author(s) 2023. CC BY 4.0 License.

Figure 3. Experiments for BA, FS and FI for MPI-ESM1.2 LGM scenario (MOD 395 ppm and LGM 185 ppm represent the realistic modern-day simulation and LGM simulation, whilst MOD 185 ppm and LGM 395 ppm represent the CO_2 and climate sensitivity experiments respectively. The ice is shown in grey). (The other experiments can be found in S3)

Under low CO_2 levels with MOD climate (MOD climate/LGM CO_2) global BA decreased by ~ 70% under all three LGM scenarios (72% for CESM1.2 and AWIESM1, 73% for MPI-ESM1.2). Despite larger global decreased BA compared to the realistic LGM scenarios, the number of grid cells in which no burning occurred was only 1.7 times higher for MPI-ESM1.2 and AWIESM1 LGM scenarios and 1.5 times CESM1.2 LGM scenario compared to the realistic MOD scenario. The spatial pattern was consistent across all three LGM scenarios, with very few grid-points showing a positive anomaly relative to the MOD experiment. Though FS increased slightly under this sensitivity experiment when burning did occur, this increase was concentrated in the tropical regions of South America and Africa (mainly Amazonia), (except for AWIESM1 were increases were observed across Eurasia). In burning grid-cells, global median FI increased by ~ 15-18% in this sensitivity experiment (18% for MPI-ESM1.2 and CESM1.2, and 15% for AWIESM1). This spatial pattern was also consistent as with BA, with very few negative anomalies, except for regions ~ 20-30°N and ~20-30°S.

Under MOD CO_2 and LGM climate, BA decreased by 41% compared to the MOD experiment for the CESM1.2 LGM scenario and by 4% for the MPI-ESM1.2 LGM scenario but increased by 48% for the AWIESM1 LGM scenario, showing a strong sensitivity to climate. The number of grid cells in which no burning occurred was of similar amplitude to the previous sensitivity experiment for the MPI-ESM1.2 and AWIESM1 LGM scenarios (~1.8 times higher compared to the realistic MOD scenario) but was much higher for the CESM1.2 LGM scenario (~3.5 increase). When burning occurred, the global median FS increased under all LGM scenarios by 17% for CESM1.2, 25% for MPI-ESM1.2 and 23% for AWIESM1. These increases were concentrated in tropical Africa, central America, and Russia, with decreases shown in North America and South Africa. Global median FI also increased under this sensitivity experiment by 2-3% for AWIESM1 and MPI-ESM1.2 but decreased by 5% for CESM1.2 LGM scenario, with decreases concentrated in Eurasia and North America.

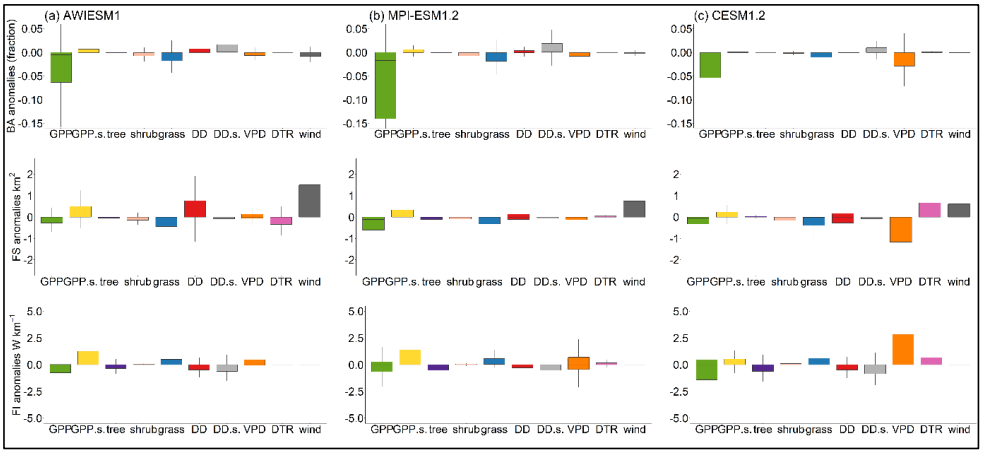

https://doi.org/10.5194/egusphere-2023-506
Preprint. Discussion started: 3 April 2023
© Author(s) 2023. CC BY 4.0 License.

Figure 4. Boxplots showing relative importance of each predictor (GPP: gross primary production, GPP.s.: GPP seasonality, tree; tree cover, shrub; shrub cover, grass; grass cover, DD: dry days, DD.s.: dry days seasonality, VPD: vapour pressure deficit, DTR: diurnal temperature range, wind: wind speed) in driving the anomaly between the MOD 395 ppm and LGM 190 ppm experiment. For each grid cell common to both experiments (on modern-day continental shelves and masking the LGM ice sheets), the predictor which caused the largest change in the anomaly between the two experiments when it was excluded from the GLM model was retained, it is the change in anomaly that is shown here. This was taken as an indicator of relative importance of that predictor in driving the observed change for (a) the AWIESM1 LGM scenario, (b) the MPI-ESM-1.2 LGM scenario and (c) the CESM1.2 LGM scenario. A positive anomaly indicates the variable caused an increase in BA, FS or FI at the LGM and a negative anomaly indicates the variable caused a decrease in BA, FS or FI at the LGM.

Reductions in BA between the MOD and LGM scenarios were driven primarily by changes in GPP, grass cover, VPD and to a lesser extent dryness (dry days (DD) and dry-day seasonality (DD.s). Changes in FI were driven by changes in GPP as well as VPD, with changes in GPP seasonality also leading to increased FI in inland regions, reflecting both changes in climate and CO_2 levels for BA and FI. Increased FS was largely driven by increased wind speeds, as well as DD and diurnal temperature range (DTR) reflecting a strong climate effect as well as GPP seasonality. Decreases in FS driven were by changes in GPP and grass cover, as well as VPD under the CESM1.2 LGM scenario and DTR under the AWIESM1 LGM scenario (Figure 4). Changes in GPP and grass cover were responsible for the largest reductions in burning, with these vegetation effects concentrated across Africa and much of Eurasia (see Figure 5). In Amazonia, changes in DD were the most important factor, reducing BA and FS (except for MPI-ESM1.2 which saw increased FS driven by DD). Increased BA in western Alaska was driven by GPP in the MPI-ESM-1.2 and AWIESM1 LGM scenarios. Increased BA in tropical regions were driven by grass cover, GPP and DD changes. Changes in VPD across the northern latitudes, especially of north America and Europe, led to decreased BA in the most conservative CESM1.2 LGM scenario. FS decreased across the Americas and Eurasia in the CESM1.2 LGM scenario because of low VPD values which reduced the occurrence of burning and offset the increases caused by wind speed and DTR in the other two LGM scenarios. Low values of VPD drove increases in FI across eastern North America, South America, western Africa, and South-East Asia.

https://doi.org/10.5194/egusphere-2023-506
Preprint. Discussion started: 3 April 2023
© Author(s) 2023. CC BY 4.0 License.

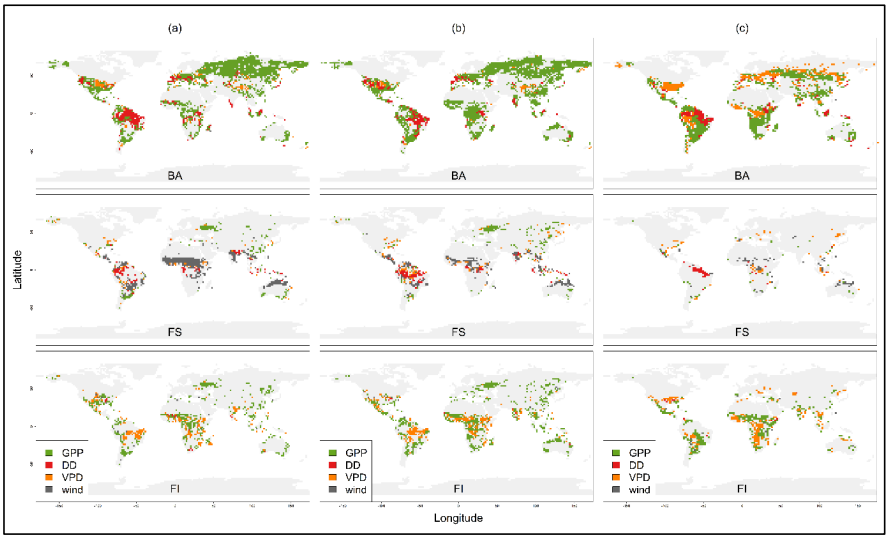

Figure 5. Map showing selection of four variables (GPP in green, DD in red, VPD in orange and wind in grey) responsible for some of the most important grid-cell drivers in reducing BA, increasing FS and FI for (a) AWIESM1 LGM scenario, (b) MPI-ESM1.2 LGM scenario and (c) CESM1.2 LGM scenario. Maps of most important grid-cell drivers for all variables and all experiments can be found in S3.

Comparing the spatial patterns of the simulated BA anomalies with charcoal-based reconstructions of the sign of changes in biomass burning (RPD; Harrison et al., 2022) showed that the best overall match occurred when both the climate and CO_2 effect were considered, with a success rate of ~ 39-45% depending on the climate scenario. The MPI-ESM1.2 and AWIESM1 LGM scenarios produced the best overall matches. None of the MOD climate/LGM CO_2 experiments identified any of the positive anomalies shown by the charcoal records. The LGM climate/MOD CO_2 experiments identified around half (~ 10-17%) of the negative anomalies identified by the realistic experiment (17-20%) and the MOD climate/LGM CO_2 sensitivity experiment, and only performed marginally better than the realistic experiment in identifying the positive anomalies (Table 3). Thus, although this sensitivity experiment produced a similar overall agreement with the reconstructions as LGM climate/LGM CO_2 simulations, only the realistic scenarios produced similar success rates for both the negative and positive anomalies. Climate change alone produced too few negative anomalies matches; CO_2 changes alone resulted in no positive anomaly matches.

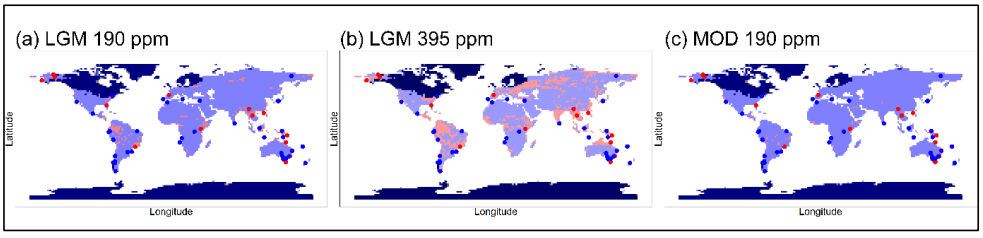

https://doi.org/10.5194/egusphere-2023-506
Preprint. Discussion started: 3 April 2023
© Author(s) 2023. CC BY 4.0 License.

Figure 6. Comparison of anomalies between the BA experiment outputs from the MPI-ESM1.2 LGM scenario with charcoal records from the Reading Palaeofire Database (RPD) for (a) the realistic LGM experiment (b) the LGM climate/MOD CO_2 sensitivity experiment and (c) the MOD climate/LGM CO_2 sensitivity experiment The modelled positive LGM-MOD anomalies are shown in red and LGM-MOD negative anomalies in blue. Dotted red (positive anomaly) and blue (negative anomaly) points show the location of the RPD records for the LGM. The LGM ice sheets are shown in dark blue.

BA experiments		MPI_ESM1.2			AWIESM1			CESM1.2 LGM		
Scenario	RPD	LGM 190	MOD 190	LGM 395	LGM 190	MOD 190	LGM 395	LGM 190	MOD 190	LGM 395
Negative RPD anomalies										
Number of records	35	20	21	13	17	21	10	20	20	17
Successful identification (percentage)		57	60	37	49	60	29	57	57	49
Positive RPD anomalies										
Number of records	16	3	0	8	6	0	5	0	0	3
Successful identification (percentage)		19	0	50	38	0	31	0	0	19
Total RPD anomalies										
Number of records	51	23	21	21	23	21	15	20	20	20
Successful identification (percentage)		45	41	41	45	41	29	39	39	39

Table 3. Comparison of sign in BA anomalies (between the MOD climate/MOD CO_2 experiment and other three experiments respectively) at the location of each RDP charcoal-based reconstruction record. A positive anomaly represents increased biomass burning, and a negative anomaly represents decreased biomass burning. A successful identification means that the sign of the experiment anomaly and the sign of the RPD charcoal-based reconstructions are the same.

The sign of the charcoal records could reflect changes in FS or FI as well as BA. However, the success rates in predicting the sign of the charcoal anomalies (both positive and negative) were somewhat worse for FS (27-31%) and FI (24-30%) than those obtained for BA for the realistic LGM experiment. Furthermore, both FS and FI did not perform any better than BA under any experiment, with the sensitivity experiments matching the charcoal anomalies slightly better for FS and FI than the realistic LGM experiment (see S4).

4. Discussion

Our simulations show a global reduction in burning at the LGM but increased median fire size and intensity when burning did occur. BA, FS and FI were all sensitive to changes in vegetation driven directly by CO_2 levels alone. BA and FI were most sensitive to this effect, with the climate effect dampening the effect of CO_2 alone when both are included. The largest reductions in burning occurred when only the CO_2 effect was

https://doi.org/10.5194/egusphere-2023-506
Preprint. Discussion started: 3 April 2023
© Author(s) 2023. CC BY 4.0 License.

considered although this experiment had fewer regions in which burning was excluded completely. This suggests that the reduction in burning was more spatially consistent and widespread under these conditions than when both effects were accounted for. The sensitivity of BA to CO_2 is explained by the reduction in fuel availability under low CO_2, a strong constraint on burnt area. For FI, including a CO_2 effect also amplified the overall global signal. This CO_2 effect is most likely driven by the negative relationship between GPP and FI fitted by the empirical model. Whilst this relationship might seem counter-intuitive, it has a sound basis. The most intense fires occur in regions with a seasonal variation in productivity rather than the most productive environments such as tropical forests (Archibald et al., 2013). High productivity can (under some climate conditions) increase the frequency of burning, which also reduces fuel loads (Rodrigues et al., 2019). Under appropriate climate conditions, there can be long-term fuel build-up in areas of low productivity that is not offset by frequent burning. All these factors help to explain why FI is not reduced at the LGM when burning occurs even though BA is. Low CO_2 decreased FS except for tropical regions and reduced the impact of climate in the realistic scenarios. We hypothesize this is because of decreased productivity leading to patchier vegetation, and hence reduced fuel continuity, which is a factor limiting wildfire spread (Dial et al., 2022; Schertzer et al., 2015).

Changes in climate alone also affected all three modelled wildfire properties. The climate effect was larger than the CO_2 effect across all models for FS, with increases in wind, DD and DTR driving the change. BA was particularly sensitive to the amplitude of climate change: climate change alone greatly reduced BA under the coldest LGM scenario (CESM1.2), had a limited effect in the intermediate LGM scenario (MPI-ESM1.2) and increased BA in the warmest LGM scenario (AWIESM1). The amplitude of change in VPD, a measure of atmospheric moisture, relative to other climate variables was especially important in influencing overall trends. In the case of BA, large decreases in VPD under the CESM1.2 climate scenario led to much more substantial reductions, most likely due to an increase in fuel moisture. Additionally, though stronger winds and increased DTR were the main drivers of larger wildfires at the LGM, low VPD values in CESM1.2 severely limited FS and FI in the northern latitudes. VPD has been shown to influence wildfire ignition and wildfire spread (Sedano & Randerson, 2014), and our results suggest high atmospheric moisture can inhibit fire spread. When vegetation was sufficiently abundant however, low VPD values were key in driving intensity. Although vegetation productivity was lower at the LGM, decreased VPD may have contributed to larger fuel build-ups, thus increasing fuel loads. This highlights the sensitivity of the fire regime not just to overall climate change but the relative amplitude of change in individual climate variables.

Our model results reproduce the global reduction of biomass burning at the LGM observed from ice cores and sedimentary charcoal records (Daniau et al., 2012; Harrison et al., 2022; Power et al., 2008; Rubino et al., 2016). Some studies have indicated the occurrence of high-intensity wildfires on the Palaeo-Agulhas Plain of South Africa, tropical regions, northern Australia, and central China at the LGM (Kraaij et al., 2020; Power et al., 2008; Rowe et al., 2021; Ruan et al., 2020; M. Song et al., 2023). Our results are consistent with the trends in these regions. The LGM simulations of BA that account for both climate and CO_2 appear to fit the charcoal records best. The spatial patterns of BA at the LGM were more consistent with the patterns shown by sedimentary charcoal records than FS and FI, consistent with the assumption that charcoal abundance can be used as a measure of biomass burning. The anomaly patterns for both FS and FI were less consistent than that of BA, suggesting a regime of less burning but larger and more intense wildfires at the LGM could be consistent with the charcoal records. Whilst FI has been reconstructed from charcoal (e.g. Duffin, 2008; Snitker, 2018) there are currently no

https://doi.org/10.5194/egusphere-2023-506
Preprint. Discussion started: 3 April 2023
© Author(s) 2023. CC BY 4.0 License.

comparable measures that record FS or FI changes globally. Charcoal records are not available from some regions, further limiting our ability to evaluate the models, particularly in Eurasia and inland South America where low CO_2 leads to large reductions in BA that are not observed when only climate is considered.

Our results are based on simple empirical models for BA, FS and FI. However, the inferred changes in BA are similar to those of Martin Calvo et al. (2015) who used the Land surface Processes and eXchanges (LPX) dynamic global vegetation model. Empirical models have been shown to perform as well as more complex process-based models in simulating burned area under modern-day conditions (Hantson et al., 2020). Thus, our conclusions about the relative impact of climate and CO_2 changes on fire properties are unlikely to be adversely affected by the relative simplicity of the models used. Their simplicity facilitates running multiple scenarios and diagnosis of the factors influencing changes in wildfire properties.

These results add to a growing body of literature highlighting the importance of considering not only changes in wildfire weather but also vegetation properties in projections of future wildfire regimes (e.g. Harrison et al., 2021; Kuhn-Régnier et al., 2021; Pausas & Keeley, 2021). The impact of rising CO_2 levels will most likely enhance vegetation growth and litter accumulation, which are important controls on fuel availability, continuity, and load. Although the trade-offs between future increases in CO_2 and reductions in productivity due to higher temperatures and atmospheric dryness are not fully understood, this work highlights the importance of considering both. These effects will most likely not be evenly distributed across the globe (Gonsamo et al., 2021; Piao et al., 2020; van der Sleen et al., 2015) and CO_2 effects may be more important in some regions than others. In fuel-limited ecosystems, CO_2 fertilization could increase fuel loads and fuel continuity, increasing overall burnt area but also the potential for larger and more intense wildfires. This is particularly worrying in regions with anticipated decreases in atmospheric moisture, especially since evidence suggests rising VPD may only counteract a small proportion of CO_2-induced plant growth (Y. Song et al., 2022). Increased woody thickening, for example in tropical South Asia (Kumar et al., 2021; Scheiter et al., 2020), may also alter fuel loads in regions that are likely to be vulnerable to ignition under a drier and warmer atmosphere (Clarke et al., 2022). This work also highlights the role of VPD in promoting fuel loads and limiting fire ignition and fire spread, a climatic variable that has been linked wildfire occurrence (Diffenbaugh et al., 2021). Although the effect of human activity was not considered in this analysis, if reductions in burnt area do contribute to greater fuel loads, suppression policies may artificially increase fuel loads in the same way reduced burnt area increased fuel loads under LGM conditions, suggesting resulting wildfires may be larger and more intense. Correctly projecting changes in fuels in the next century will require considering both the effect of VPD and effects of CO_2 on plant growth and fuel loads.

Our results stress the importance of accounting for the effects of CO_2 on vegetation when considering how future fire regimes may evolve. Different aspects of the fire regime respond differently to changes in fuel properties. Without accounting for this crucial effect, our understanding of future risks will remain limited.

Code availability. All code used in this paper is available at freely available for use in RStudio: the code for the GLM models is available at https://doi.org/10.6084/m9.figshare.19071044.v1, and the code to generate the experiments are available at: https://doi.org/10.6084/m9.figshare.22285303.v2 and https://doi.org/10.6084/m9.figshare.22285279.v2.

https://doi.org/10.5194/egusphere-2023-506
Preprint. Discussion started: 3 April 2023
© Author(s) 2023. CC BY 4.0 License.

Data availability: All LGM data can be retrieved from https://esgf-node.llnl.gov/projects/cmip6/, all modern data can be retrieved from references provided. The P Model documentation is available at https://pyrealm.readthedocs.io/en/latest/ and the BIOME4 documentation is available at https://pmip2.lsce.ipsl.fr/synth/biome4.shtml and https://github.com/jedokaplan/BIOME4.

Author contributions. Experiments conception, strategy and interpretation were developed by O H, ICP and SPH jointly. OH performed the data processing and analysis, and produced the graphics and Tables. OH wrote the original draft; SPH and ICP contributed to the final draft.

Competing interests. The contact author has declared that neither themselves nor any other authors have a conflict of interest.

Acknowledgements and financial support. OH acknowledges support from the NERC Centre for Doctoral Training in Quantitative and Modelling skills in Ecology and Evolution (Grant No. NE/S007415/1) and from the Leverhulme Trust through the Leverhulme Centre for Wildfires, Environment and Society (Grant No. RC-2018-023). ICP acknowledges support from the European Research Council (787203 REALM) under the European Union's Horizon 2020 research programme. SPH is supported by the European Research Council (694481 GC2.0) under the same programme. This work is a contribution to the LEMONTREE (Land Ecosystem Models based On New Theory, obseRvations and ExperimEnts) project, funded through the generosity of Eric and Wendy Schmidt by recommendation of the Schmidt Futures program.

References

Abatzoglou, J. T., Williams, A. P., & Barbero, R. (2019). Global emergence of anthropogenic climate change in fire weather indices. *Geophysical Research Letters*, *46*(1), 326–336.

Albani, S., Balkanski, Y., Mahowald, N., Winckler, G., Maggi, V., & Delmonte, B. (2018). Aerosol-climate interactions during the Last Glacial Maximum. In *Current Climate Change Reports* (Vol. 4, Issue 2, pp. 99–114). Springer. https://doi.org/10.1007/s40641-018-0100-7

Andela, N., Morton, D. C., Giglio, L., Paugam, R., Chen, Y., Hantson, S., Van Der Werf, G. R., & Randerson, J. T. (2019). The Global Fire Atlas of individual fire size, duration, speed and direction. *Earth System Science Data*, *11*(2), 529–552.

Archibald, S., Lehmann, C. E. R., Gómez-Dans, J. L., & Bradstock, R. A. (2013). Defining pyromes and global syndromes of fire regimes. *Proceedings of the National Academy of Sciences*, *110*(16), 6442–6447.

Betts, R. A., Golding, N., Gonzalez, P., Gornall, J., Kahana, R., Kay, G., Mitchell, L., & Wiltshire, A. (2015). Climate and land use change impacts on global terrestrial ecosystems and river flows in the HadGEM2-ES Earth system model using the representative concentration pathways. *Biogeosciences*, *12*(5), 1317–1338.

Bond, W. J., & Midgley, G. F. (2012). Carbon dioxide and the uneasy interactions of trees and savannah grasses. *Philosophical Transactions of the Royal Society B: Biological Sciences*, *367*(1588), 601–612.

Bond, W. J., Midgley, G. F., & Woodward, F. I. (2003). The importance of low atmospheric CO_2 and fire in promoting the spread of grasslands and savannas. *Global Change Biology*, *9*(7), 973–982.

https://doi.org/10.5194/egusphere-2023-506
Preprint. Discussion started: 3 April 2023
© Author(s) 2023. CC BY 4.0 License.

Bowman, D. M. J. S., Kolden, C. A., Abatzoglou, J. T., Johnston, F. H., van der Werf, G. R., & Flannigan, M. (2020). Vegetation fires in the Anthropocene. *Nature Reviews Earth & Environment*, *1*(10), 500–515.

Bradstock, R. A. (2010). A biogeographic model of fire regimes in Australia: current and future implications. *Global Ecology and Biogeography*, *19*(2), 145–158.

Bragg, F. J., Prentice, I. C., Harrison, S. P., Eglinton, G., Foster, P. N., Rommerskirchen, F., & Rullkötter, J. (2013). Stable isotope and modelling evidence for CO_2 as a driver of glacial–interglacial vegetation shifts in southern Africa. *Biogeosciences*, *10*(3), 2001–2010.

Buitenwerf, R., Bond, W. J., Stevens, N., & Trollope, Wsw. (2012). Increased tree densities in South African savannas:> 50 years of data suggests CO_2 as a driver. *Global Change Biology*, *18*(2), 675–684.

Clarke, H., Nolan, R. H., de Dios, V. R., Bradstock, R., Griebel, A., Khanal, S., & Boer, M. M. (2022). Forest fire threatens global carbon sinks and population centres under rising atmospheric water demand. *Nature Communications*, *13*(1), 7161. https://doi.org/10.1038/s41467-022-34966-3

Cucchi, M., Weedon, G. P., Amici, A., Bellouin, N., Lange, S., Müller Schmied, H., Hersbach, H., & Buontempo, C. (2020). WFDE5: bias-adjusted ERA5 reanalysis data for impact studies. *Earth System Science Data*, *12*(3), 2097–2120.

Daniau, A.-L., Bartlein, P.J., Harrison, S.P., Prentice, I.C., Brewer, S., Friedlingstein, P., Harrison-Prentice, T.I., Inoue, J., Marlon, J.R., Mooney, S., Power, M.J., Stevenson, J., Tinner, W., Andrič, M., Atanassova, J., Behling, H., Black, M., Blarquez, O., Brown, K. J., Carcaillet, C., Colhoun, E., Colombaroli, D., Davis, B.A.S., D'Costa, D., Dodson, J., Dupont, L., Eshetu, Z., Gavin, D.G., Genries, A., Gebru, T., Haberle, S., Hallett, D. J., Horn, S., Hope, G., Katamura, F., Kennedy, L., Kershaw, P., Krivonogov, S., Long, C., Magri, D., Marinova, E., McKenzie, G.M., Moreno, P.I., Moss, P., Neumann, F.H., Norström, E., Paitre, C., Rius, D., Roberts, N., Robinson, G., Sasaki, N., Scott, L., Takahara, H., Terwilliger, V., Thevenon, F., Turner, R.B., Valsecchi, V.G., Vannière, B., Walsh, M., Williams, N., & Zhang, Y. (2012). Predictability of biomass burning in response to climate changes. *Global Biogeochemical Cycles* 26: GB4007, doi:10.1029/2011GB004249.

Dial, R. J., Maher, C. T., Hewitt, R. E., & Sullivan, P. F. (2022). Sufficient conditions for rapid range expansion of a boreal conifer. *Nature*, *608*(7923), 546–551. https://doi.org/10.1038/s41586-022-05093-2

Diffenbaugh, N. S., Konings, A. G., & Field, C. B. (2021). Atmospheric variability contributes to increasing wildfire weather but not as much as global warming. *Proceedings of the National Academy of Sciences*, *118*(46), e2117876118. https://doi.org/10.1073/pnas.2117876118

Donohue, R. J., Roderick, M. L., McVicar, T. R., & Farquhar, G. D. (2013). Impact of CO_2 fertilization on maximum foliage cover across the globe's warm, arid environments. *Geophys. Res. Lett.*, *40*, 3031–3035. https://doi.org/10.1002/grl.50563

Duffin, K. I. (2008). The representation of rainfall and fire intensity in fossil pollen and charcoal records from a South African savanna. *Review of Palaeobotany and Palynology*, *151*(1–2), 59–71.

Flannigan, M., Cantin, A. S., De Groot, W. J., Wotton, M., Newbery, A., & Gowman, L. M. (2013). Global wildland fire season severity in the 21st century. *Forest Ecology and Management*, *294*, 54–61.

Fuller, D. Q., Denham, T., Arroyo-Kalin, M., Lucas, L., Stevens, C. J., Qin, L., Allaby, R. G., & Purugganan, M. D. (2014). Convergent evolution and parallelism in plant domestication revealed by an expanding archaeological record. *Proceedings of the National Academy of Sciences*, *111*(17), 6147–6152.

https://doi.org/10.5194/egusphere-2023-506
Preprint. Discussion started: 3 April 2023
© Author(s) 2023. CC BY 4.0 License.

Gonsamo, A., Ciais, P., Miralles, D. G., Sitch, S., Dorigo, W., Lombardozzi, D., Friedlingstein, P., Nabel, J. E. M. S., Goll, D. S., & O'Sullivan, M. Arneth, A., Anthoni, P., Jain, A.K., Wiltshire A., Peylin P., Cescatti A. (2021). Greening drylands despite warming consistent with carbon dioxide fertilization effect. *Global Change Biology*, *27*(14), 3336–3349.

Haas, O., Prentice, I. C., & Harrison, S. P. (2022). Global environmental controls on wildfire burnt area, size, and intensity. *Environmental Research Letters*, *17*(6), 065004.

Haas, Olivia (2023): Scripts and input files. figshare. Dataset. https://doi.org/10.6084/m9.figshare.19071044.v1

Haas, Olivia (2023): Data for: The response of wildfire regimes to Last Glacial Maximum carbon dioxide and climate. figshare. Dataset. https://doi.org/10.6084/m9.figshare.22285303.v2

Haas, Olivia (2023): R scripts to run models for: The response of wildfire regimes to Last Glacial Maximum carbon dioxide and climate. figshare. Software. https://doi.org/10.6084/m9.figshare.22285279.v2

Hantson, S., Kelley, D. I., Arneth, A., Harrison, S. P., Archibald, S., Bachelet, D., Forrest, M., Hickler, T., Lasslop, G., Li, F., Mangeon, S., Melton, J.R., Nieradzik, L., Rabin, S.S., Prentice, I.C., Sheehan, T., Sitch, S., Teckentrup, L., Voulgarakis, A., & Yue, C. (2020). Quantitative assessment of fire and vegetation properties in simulations with fire-enabled vegetation models from the Fire Model Intercomparison Project. *Geoscientific Model Development*, *13*(7), 3299–3318.

Harrison, S. P., & Prentice, C. I. (2003). Climate and CO_2 controls on global vegetation distribution at the last glacial maximum: analysis based on palaeovegetation data, biome modelling and palaeoclimate simulations. *Global Change Biology*, *9*(7), 983–1004.

Harrison, S. P., Prentice, I. C., Bloomfield, K. J., Dong, N., Forkel, M., Forrest, M., Ningthoujam, R. K., Pellegrini, A., Shen, Y., & Baudena, M. Cardoso, A.W., Huss, J.C., Joshi J., Oliveras, I., Pausas, J.G. and Simpson, J.K. (2021). Understanding and modelling wildfire regimes: an ecological perspective. *Environmental Research Letters*, *16*(12), 125008.

Harrison, S.P., Villegas-Diaz, R., Cruz-Silva, E., Gallagher, D., Kesner, D., Lincoln, P., Shen, Y., Sweeney, L., Colombaroli, D., Ali, A., Barhoumi, C., Bergeron, Y., Blyakharchuk, T., Bobek, P., Bradshaw, R., Clear, J.L., Czerwiński, S., Daniau, A-L., Dodson, J., Edwards, K.J., Edwards, M.E., Feurdean, A., Foster, D., Gajewski, K., Gałka, M., Garneau, M., Giesecke, T., Gil Romera, G., Girardin, M.P., Hoefer, D., Huang, K., Inoue, J., Jamrichová, E., Jasiunas, N., Jiang, W., Jiménez-Moreno, G., Karpińska-Kołaczek, M., Kołaczek, P., Kuosmanen, N., Lamentowicz, M., Lavoie, M., Li, F., Li, J., Lisitsyna, O., López-Sáez, J.A., Luelmo-Lautenschlaeger, R., Magnan, G., Magyari, E.K., Maksims, A., Marcisz, K., Marinova, E., Marlon, J., Mensing, S., Miroslaw-Grabowska, J., Oswald, W., Pérez-Díaz, S., Pérez-Obiol, R., Piilo, S., Poska, A., Qin, X., Remy, C.C., Richard, P.J.H., Salonen, S., Sasaki, N., Schneider, H., Shotyk, W., Stancikaite, M., Šteinberga, D., Stivrins, N., Takahara, H., Tan, Z., Trasune, L., Umbanhowar, C.E., Väliranta, M., Vassiljev, J., Xiao, X., Xu, Q., Xu, X., Zawisza, E., Zhao, Y., Zhou, Z., & Paillard, J. (2022). The Reading Palaeofire database: an expanded global resource to document changes in fire regimes from sedimentary charcoal records *Earth System Science Data* 14: 1109-1124 https://doi.org/10.5194/essd-14-1109-2022

Humber, M. L., Boschetti, L., Giglio, L., & Justice, C. O. (2019). Spatial and temporal intercomparison of four global burned area products. *International Journal of Digital Earth*, *12*(4), 460–484.

https://doi.org/10.5194/egusphere-2023-506
Preprint. Discussion started: 3 April 2023
© Author(s) 2023. CC BY 4.0 License.

Jolly, W. M., Cochrane, M. A., Freeborn, P. H., Holden, Z. A., Brown, T. J., Williamson, G. J., & Bowman, D. M. J. S. (2015). Climate-induced variations in global wildfire danger from 1979 to 2013. *Nature Communications*, *6*(1), 1–11.

Kageyama, M., Harrison S.P., Kapsch, M.L, Lofverstrom, M., Lora J.M., Mikolajewicz U., Sherriff-Tadano,S., Vadsaria T., Abe-Ouchi A., Bouttes N., Chandan, D., Gregoire L.J., Ivanovic, R.F., Kenji Izumi, Allegra N. LeGrande, Fanny Lhardy, Gerrit Lohmann, Polina A. Morozova, Rumi Ohgaito, Paul, Peltier W.R., Poulsen, C.J., Quiquet, A., Roche, D.M., Shi, X., Tierney, J.E., Valdes, P.J., Volodin E. & Zhu J. (2021). The PMIP4-CMIP6 Last Glacial Maximum experiments: preliminary results and comparison with the PMIP3-CMIP5 simulations. *Climate of the Past* 17: 1065-1089

Kaplan, J.O., Bigelow, Prentice, I.C., Harrison, S.P., P.J., N.H., Bartlein, Christensen, T.R., Cramer, W., Matveyeva, N.V., McGuire, A.D., Murray, D.F., Razzhivin, V.Y., Smith, B. and Walker, D.A., Anderson, P.M., Andreev, A.A., Brubaker, L.B., Edwards, M.E., & Lozhkin, A.V. (2003). Climate change and Arctic ecosystems II: Modeling, palaeodata-model comparisons, and future projections. *Journal of Geophysical Research-Atmosphere* 108, No. D19, 8171. (DOI: 10.1029/2002JD002559).

Kaplan, J. O., Pfeiffer, M., Kolen, J. C. A., & Davis, B. A. S. (2016). Large scale anthropogenic reduction of forest cover in Last Glacial Maximum Europe. *PLoS One*, *11*(11), e0166726.

Kgope, B. S., Bond, W. J., & Midgley, G. F. (2010). Growth responses of African savanna trees implicate atmospheric [CO2] as a driver of past and current changes in savanna tree cover. *Austral Ecology*, *35*(4), 451–463.

Knorr, W., Jiang, L., & Arneth, A. (2016). Climate, CO_2 and human population impacts on global wildfire emissions. *Biogeosciences*, *13*(1), 267–282.

Kraaij, T., Engelbrecht, F., Franklin, J., & Cowling, R. M. (2020). A fiery past: A comparison of glacial and contemporary fire regimes on the Palaeo-Agulhas Plain, Cape Floristic Region. *Quaternary Science Reviews*, *235*, 106059.

Kuhn-Régnier, A., Voulgarakis, A., Nowack, P., Forkel, M., Prentice, I. C., & Harrison, S. P. (2021). The importance of antecedent vegetation and drought conditions as global drivers of burnt area. *Biogeosciences*, *18*(12), 3861–3879.

Kumar, D., Pfeiffer, M., Gaillard, C., Langan, L., & Scheiter, S. (2021). Climate change and elevated CO_2 favor forest over savanna under different future scenarios in South Asia. *Biogeosciences*, *18*(9), 2957–2979.

Li, F., Levis, S., & Ward, D. S. (2013). Quantifying the role of fire in the Earth system - Part 1: Improved global fire modeling in the Community Earth System Model (CESM1). *Biogeosciences*, *10*(4), 2293–2314. https://doi.org/10.5194/bg-10-2293-2013

Li, W., MacBean, N., Ciais, P., Defourny, P., Lamarche, C., Bontemps, S., Houghton, R. A., & Peng, S. (2018). Gross and net land cover changes in the main plant functional types derived from the annual ESA CCI land cover maps (1992–2015). *Earth System Science Data*, *10*(1), 219–234.

Lohmann, G., Butzin, M., Eissner, N., Shi, X., & Stepanek, C. (2020). Abrupt climate and weather changes across time scales. *Paleoceanography and Paleoclimatology*, *35*(9), e2019PA003782.

Marlon, J. R., Kelly, R., Daniau, A.-L., Vannière, B., Power, M. J., Bartlein, P., Higuera, P., Blarquez, O., Brewer, S., Brücher, T, Feurdean A., Romera G.G., Iglesias V., Maezumi S.Y., Magi, B., Courtney Mustaphi, C.J.,

https://doi.org/10.5194/egusphere-2023-506
Preprint. Discussion started: 3 April 2023
© Author(s) 2023. CC BY 4.0 License.

& Zhihai, T. (2016). Reconstructions of biomass burning from sediment-charcoal records to improve data–model comparisons. *Biogeosciences*, *13*(11), 3225–3244.

Martin Calvo, M., & Prentice, I. C. (2015). Effects of fire and CO_2 on biogeography and primary production in glacial and modern climates. *New Phytologist*, *208*(3), 987–994.

Martin Calvo, M., Prentice, I. C., & Harrison, S. P. (2014). Climate versus carbon dioxide controls on biomass burning: a model analysis of the glacial–interglacial contrast. *Biogeosciences*, *11*(21), 6017–6027.

Mauritsen, T., Bader, J., Becker, T., Behrens, J., Bittner, M., Brokopf, R., Brovkin, V., Claussen, M., Crueger, T., Esch, M., Fast I., Fiedler S., Fläschner D., Gayler V., Giorgetta M., Goll D.S., Haak H., Hagemann S., Hedemann C., Hohenegger C., Ilyina, T., Jahns T., Jimenéz-de-la-Cuesta, D., Jungclaus J., Kleinen T., Kloster S., Kracher D., Kinne S., Kleberg D., Lasslop G., Kornblueh L., Marotzke J., Matei D., Meraner K., Mikolajewicz U., Modali K., Möbis, B., Müller A.W., Julia E. M. S. Nabel, J.E. M. S, Nam C.C.W., Notz D., Nyawira S., Paulsen H., Peters K., Pincus R., Pohlmann H., Pongratz J., Popp M., Jürgen Raddatz T., Rast S., Redler,R., Reick, C.H., Rohrschneider, T., Schemann V., Schmidt, H., Schnur R., Schulzweida, U., Six K.D., Stein, L., Stemmler, I., Stevens B., Storch J-S.V, Tian F., Voigt, A., Vrese, P., Wieners K., Wilkenskjeld, S., Winkler A., Roeckner, E. (2019). Developments in the MPI-M Earth System Model version 1.2 (MPI-ESM1. 2) and its response to increasing CO_2. *Journal of Advances in Modeling Earth Systems*, *11*(4), 998–1038.

Moreno, P. I., Videla, J., Valero-Garcés, B., Alloway, B. v, & Heusser, L. E. (2018). A continuous record of vegetation, fire-regime and climatic changes in northwestern Patagonia spanning the last 25,000 years. *Quaternary Science Reviews*, *198*, 15–36.

Pausas, J. G. (2015). Bark thickness and fire regime. *Functional Ecology*, *29*(3), 315–327.

Pausas, J. G., & Keeley, J. E. (2021). Wildfires and global change. *Frontiers in Ecology and the Environment*, *19*(7), 387–395.

Pausas, J. G., & Ribeiro, E. (2013). The global fire–productivity relationship. *Global Ecology and Biogeography*, *22*(6), 728–736.

Peltier, W. R., Argus, D. F., & Drummond, R. (2015). Space geodesy constrains ice age terminal deglaciation: The global ICE-6G_C (VM5a) model. *Journal of Geophysical Research: Solid Earth*, *120*(1), 450–487.

Piao, S., Wang, X., Park, T., Chen, C., Lian, X. U., He, Y., Bjerke, J. W., Chen, A., Ciais, P., Tømmervik, H., Nemani R.R. & Myneni R.B. (2020). Characteristics, drivers and feedbacks of global greening. *Nature Reviews Earth & Environment*, *1*(1), 14–27.

Power, M.J., Ortiz, N., Marlon, J., Bartlein, P.J., Harrison, S.P., Mayle, F., Ballouche, A., Bradshaw, R., Carcaillet, C., Cordova, C., Mooney, S., Moreno, P., Prentice, I.C., Thonicke, K., Tinner, W., Whitlock, C., Zhang, Y., Zhao, Y., Anderson, R.S., Beer, R., Behling, H., Briles, C., Brown, K, Brunelle A., Bush, M., Clark, J., Colombaroli, D., Chu, C. Q., Daniels, M., Dodson, J., Edwards, M.E., Fisinger, W., Gavin, D.G., Gobet, E., Hallett, D.J., Higuera, P., Horn, S., Inoue, J., Kaltenrieder, P., Kennedy, L., Kong, Z.C., Long, C., Lynch, J., Lynch, B., McGlone, M., Meeks, S., Meyer, G., Minckley, T., Mohr, J., Noti, R., Pierce, J., Richard, P., Shuman, B.J., Takahara, H., Toney, J., Turney, C., Umbanhower, C., Vandergoes, M., Vanniere, B., Vescovi, E., Walsh, M., Wang, X., Williams, N., Wilmshurst, J., & Zhang , J.H. (2008). Changes in fire regimes since the Last Glacial Maximum: an assessment based on a global synthesis and analysis of charcoal data. *Climate Dynamics*, *30*(7), 887–907.

https://doi.org/10.5194/egusphere-2023-506
Preprint. Discussion started: 3 April 2023
© Author(s) 2023. CC BY 4.0 License.

Rodrigues, M., Costafreda-Aumedes, S., Comas, C., & Vega-García, C. (2019). Spatial stratification of wildfire drivers towards enhanced definition of large-fire regime zoning and fire seasons. *Science of the Total Environment*, *689*, 634–644.

Rogers, B. M., Balch, J. K., Goetz, S. J., Lehmann, C. E. R., & Turetsky, M. (2020). Focus on changing fire regimes: interactions with climate, ecosystems, and society. *Environmental Research Letters*, *15*(3), 030201.

Rowe, C., Wurster, C. M., Zwart, C., Brand, M., Hutley, L. B., Levchenko, V., & Bird, M. I. (2021). Vegetation over the last glacial maximum at Girraween Lagoon, monsoonal northern Australia. *Quaternary Research*, *102*, 39–52.

Ruan, Y., Mohtadi, M., Dupont, L. M., Hebbeln, D., van der Kaars, S., Hopmans, E. C., Schouten, S., Hyer, E. J., & Schefuß, E. (2020). Interaction of fire, vegetation, and climate in tropical ecosystems: A multiproxy study over the past 22,000 years. *Global Biogeochemical Cycles*, *34*(11), e2020GB006677.

Rubino, M., D'Onofrio, A., Seki, O., & Bendle, J. A. (2016). Ice-core records of biomass burning. *The Anthropocene Review*, *3*(2), 140–162.

Scheiter, S., Kumar, D., Corlett, R. T., Gaillard, C., Langan, L., Lapuz, R. S., Martens, C., Pfeiffer, M., & Tomlinson, K. W. (2020). Climate change promotes transitions to tall evergreen vegetation in tropical Asia. *Global Change Biology*, *26*(9), 5106–5124.

Schertzer, E., Staver, A. C., & Levin, S. A. (2015). Implications of the spatial dynamics of fire spread for the bistability of savanna and forest. *Journal of Mathematical Biology*, *70*(1), 329–341. https://doi.org/10.1007/s00285-014-0757-z

Sedano, F., & Randerson, J. T. (2014). Multi-scale influence of vapor pressure deficit on fire ignition and spread in boreal forest ecosystems. *Biogeosciences*, *11*(14), 3739–3755. https://doi.org/10.5194/bg-11-3739-2014

Sidorenko, D., Rackow, T., Jung, T., Semmler, T., Barbi, D., Danilov, S., Dethloff, K., Dorn, W., Fieg, K., Gößling, H. F., Handorf, D., Harig S., Hiller W., Juricke S., Losch M., Schröter J., Sein D.V. & Wang Q. (2015). Towards multi-resolution global climate modeling with ECHAM6–FESOM. Part I: model formulation and mean climate. *Climate Dynamics*, *44*, 757–780.

Snitker, G., (2018). Identifying natural and anthropogenic drivers of prehistoric fire regimes through simulated charcoal records. *Journal of Archaeological Science*, *95*, 1–15.

Song, M., Dodson, J., Lu, F., Shi, G., & Yan, H. (2023). A continuous paleorecord of vegetation and environmental change from Erxianyan Wetland over the past 60,000 years in central China. *Palaeogeography, Palaeoclimatology, Palaeoecology*, 111399.

Song, Y., Jiao, W., Wang, J., & Wang, L. (2022). Increased global vegetation productivity despite rising atmospheric dryness over the last two decades. *Earth's Future*, *10*(7). https://doi.org/10.1029/2021EF002634

Stocker, B. D., Wang, H., Smith, N. G., Harrison, S. P., Keenan, T. F., Sandoval, D., Davis, T., & Prentice, I. C. (2020). P-model v1. 0: an optimality-based light use efficiency model for simulating ecosystem gross primary production. *Geoscientific Model Development*, *13*(3), 1545–1581.

Tierney, J. E., Zhu, J., King, J., Malevich, S. B., Hakim, G. J., & Poulsen, C. J. (2020). Glacial cooling and climate sensitivity revisited. *Nature*, *584*(7822), 569–573.

https://doi.org/10.5194/egusphere-2023-506
Preprint. Discussion started: 3 April 2023
© Author(s) 2023. CC BY 4.0 License.

van der Sleen, P., Groenendijk, P., Vlam, M., Anten, N. P. R., Boom, A., Bongers, F., Pons, T. L., Terburg, G., & Zuidema, P. A. (2015). No growth stimulation of tropical trees by 150 years of CO_2 fertilization but water-use efficiency increased. *Nature Geoscience*, *8*(1), 24–28. https://doi.org/10.1038/ngeo2313

Wang, H., Prentice, I. C., Keenan, T. F., Davis, T. W., Wright, I. J., Cornwell, W. K., Evans, B. J., & Peng, C. (2017). Towards a universal model for carbon dioxide uptake by plants. *Nature Plants*, *3*(9), 734–741.